A Numerical Method for the Calculation of Image Aberrations of Inhomogeneous Magnetic Sector Fields Between Conical Pole Faces

F. Rüdenauer und F. P. Viehböck

I. Physikalisches Institut der Universität Wien, and Physik-Institut, Reaktorzentrum Seibersdorf, Österr. Studiengesellschaft für Atomenergie, G.m.b.H., Austria

(Z. Naturforschg. **21 a**, 2—8 [1966]; received 2 August 1965)

Dedicated to Prof. J. Mattauch *on his 70th birthday*

Owing to their increased dispersion magnetic analysers with inhomogeneous magnetic fields may be useful for various applications e. g. nuclear spectroscopy, mass spectroscopy, and isotope separation. This inhomogeneity may be aquired by conically shaped pole faces. Boerboom and Tasman gave an analytical treatment of these fields, which allows the calculation of aberrations for particles along the medium radius. For some applications e. g. simultaneous collection of more isotopes in an isotope separator it would be important to know how the quality of focus varies with increasing distance from the mean radius. In this paper a numerical method is described which allows a three dimensional ray-tracing throughout inhomogeneous magnetic sector fields. Some of the results have been published elsewhere [1].

The ion-optical properties as well as the image aberrations for the classical mass spectroscopic arrangements using homogeneous magnetic sector fields were calculated by Hintenberger et al. [2]. Increased dispersion, which in many cases corresponds to increased resolution, is achieved by inhomogeneous fields. Detailed mathematical treatment for such fields is given by Svartholm and Siegbahn [3] and Tasman and Boerboom [4].

The finite image width of an idealized point or line source is mainly caused by the generally poor focusing of the marginal rays in a homogeneous field. Giving the field strength on both sides of the circular median ion path a somewhat lower value by specially shaped pole faces or by appropriate shimming results in a much narrower focus. In other terms, if a given width of focus can be tolerated, rather wide angles may be accepted which means that such an instrument has higher luminosity compared with the homogeneous field machine. The required field shape was calculated by Beiduk and Konopinsky [5] and was applicated by Kistemaker and Zilverschoon [6] for the construction of a large 1 m radius machine. Since the condition of maximum field strength along the axis of the beam is fulfilled for the mean radius only, it is evident that the Beiduk–Konopinski field gives second order focusing for one mass only.

Another possibility to avoid interference from neighbouring masses and so to increase the purity of separated isotopes is the introduction of a radial field gradient along the mean radius. This results in an increased distance between the focal patterns of adjacent masses which is also convenient for the construction of collecting devices, especially in the high mass region. Such an instrument has first been built by Alekseevski [7]. The required field shape may be achieved by conically shaped pole faces which provide a radially decreasing magnetic field. On a small 20 cm radius machine with conical pole faces Tasman was able to demonstrate that a tenfold increase in resolution is possible compared with a homogeneous machine with same mean radius. Moreover, by a special choice of the remaining parameters such as deflecting angle and angle of entrance and exit of the field some aberrations may be corrected for. Again in this case, analytical calculation of aberrations for other than the circular median trajectory is rather complicated since in those other cases the field coefficients are not independent from

[1] F. Rüdenauer and F. P. Viehböck, Nucl. Instr. Methods **37** [1965], in press.
[2] H. Hintenberger, H. Wende, and L. A. König, Z. Naturforschg. **10 a**, 605 [1955].
[3] N. Svartholm and K. Siegbahn, Arkiv Astron. Mat. Fys. **33 A**, No. 21 [1946].
[4] H. A. Tasman and A. J. H. Boerboom, Z. Naturforschg. **14 a**, 121, 818, 822 [1959].
[5] F. M. Beiduk and E. J. Konopinski, Rev. Sci. Instr. **19**, 594 [1948].
[6] C. J. Zilverschoon, Thesis, University of Amsterdam 1954.
[7] N. Alekseevski, Dokl. Akad. Nauk SSSR **100**, 229.

the azimuthal angle. Especially in the field of isotope separation where one wants to collect more isotopes simultaneously it is important to know how the quality of focus varies with increasing distance from the mean path. For this purpose a three-dimensional numerical ray tracing method seems appropriate.

I. Method

Numerical calculations may be performed in two ways. The shape of the magnetic field between the pole faces may be given by an analytical formula or by a carefully measured field plot which may also include the stray fields. In this paper we chose the first method because it is more generally applicable and gives good agreement with actual conditions if the pole gaps are not too wide and the iron is not in saturation.

I.1. Magnetic Field Shape between Conical Pole Faces

A magnetic field with rotational symmetry which is also symmetric to the plane $v=0$ may be represented by expanding the scalar magnetic potential into a power series [4]:

$$\varphi_m/B = a_1 v + a_2 u v + a_3 u^2 v + a_4 v^3 + a_5 u^3 v + a_6 u v^3 + a_7 u^4 v + a_8 u^2 v^3 + a_9 v^5 + \dots \quad (1)$$

where

$$\begin{aligned} a_1 &= -1, \\ a_2 &= n, \\ a_3 &= \tfrac{1}{2}[X(1-n) - 2n], \\ a_4 &= -\tfrac{1}{6}[X(1-n) - n], \\ a_5 &= -C_3, \\ a_6 &= [\tfrac{1}{2} n - \tfrac{1}{6} X(1-n) + C_3], \\ a_7 &= -C_4, \\ a_8 &= [-\tfrac{1}{2} n + \tfrac{1}{6} X(1-n) + \tfrac{1}{2} C_3 + 2 C_4], \\ a_9 &= [\tfrac{1}{40} n - \tfrac{1}{120} X(1-n) - \tfrac{1}{10} C_3 - \tfrac{1}{5} C_4]. \end{aligned}$$

B is the absolute value of the axial magnetic field strength along the circle $u=0$, $v=0$, and φ_m is normalized such that $\varphi_m = 0$ in the median plane $v=0$. The coordinate system used is shown in fig. 1.

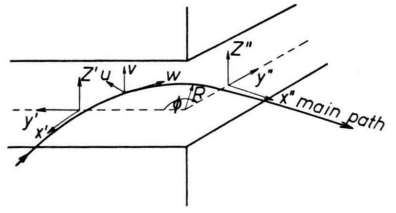

Fig. 1. Coordinate System.

In the special case of a conical pole-shoe profile (fig. 2)

$$v = a u + b,$$

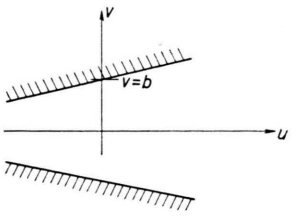

Fig. 2. Pole-Shoe Profile.

one obtains for a, C_3, C_4, X [8]

$$\begin{aligned} a &= n\,b + \tfrac{1}{6} n(1-n)\, b^3 + \dots, \\ X &= 2n + \tfrac{1}{3} n(1-n)\, b^2 + \dots, \\ C_3 &= -n^3 + \tfrac{1}{6} n(1-n)^2\,(1+2n)\, b^2 + \dots, \\ C_4 &= n^4 - \tfrac{1}{6} n(1-n)^2\,(1+2n+3n^2)\, b^2 + \dots . \end{aligned} \quad (2)$$

The magnetic vector potential is chosen so that the only non-vanishing component is the azimuthal component A_w. Up to terms of fifth order, A is represented by the power series

$$\begin{aligned} A_w/B = {} & b_0 + b_1 u + b_2 u^2 + b_3 v^2 + b_4 u^3 + b_5 u v^2 \\ & + b_6 u^4 + b_7 u^2 v^2 + b_8 v^4 \\ & + b_9 u^5 + b_{10} u^3 v^2 + b_{11} u v^4 + \dots \end{aligned} \quad (3)$$

with

$$\begin{aligned} b_0 &= \tfrac{1}{2}, & b_4 &= -\tfrac{1}{3}(B_1 + B_2), \\ b_1 &= \tfrac{1}{2}, & b_5 &= \tfrac{1}{2}(B_1 + 2B_2), \\ b_2 &= B_1/2, & b_6 &= \tfrac{1}{24}(5B_1 + 2B_2 + B_3), \\ b_3 &= -B_1/2, & b_7 &= -\tfrac{1}{4} B_3, \\ b_8 &= -\tfrac{1}{12}(B_1 + B_2 - \tfrac{1}{2} B_3), \\ b_9 &= -\tfrac{1}{120}(25B_1 + 10B_2 + B_3 - 24C_4), \\ b_{10} &= -2C_4, \\ b_{11} &= \tfrac{1}{24}(4B_1 + 4B_2 + B_3 + 24C_4) \end{aligned}$$

where

$$B_1 = -n, \quad B_2 = \tfrac{1}{2}[X(1-n) - n], \quad B_3 = 6C_3.$$

The components of the magnetic field strength may be expressed by the magnetic scalar potential and the vector potential, respectively [9],

$$\begin{aligned} B_u &= \frac{\partial \varphi_m}{\partial u} = \frac{\partial A_w}{\partial v}, \\ B_v &= -\frac{\partial \varphi_m}{\partial v} = \frac{1}{1+u}\frac{\partial}{\partial u}[(1+u)\, A_w]. \end{aligned} \quad (4)$$

[8] A. J. H. Boerboom, H. A. Tasman, and H. Wachsmuth, Z. Naturforschg. **14 a**, 816 [1959].

[9] H. Grümm, Acta Phys. Austr. **8**, 119 [1953].

B_u and B_v may be expanded into power series:

$$B_u = B_1 v - (B_1 + 2B_2)\, u v + \dots ,$$
$$B_v = B + B_1 u - (\tfrac{1}{2} B_1 + B_2)\, u^2 + B_2 v^2 + \dots .$$

I.2. The Equations of Motion

The equations of motion for a charged particle in a purely magnetic field expressed in cylindrical coordinates (r, z, ψ) [10] are

$$m z'' = -e[C/r + (e/m) A]\, \partial A/\partial z ,$$
$$m r'' = -e[C/r + (e/m) A]\, [-C m/(e r^2) + \partial A/\partial r],$$
$$r^2 \psi' = C + (e/m)\, A , \qquad (5)$$

where $C = r_0^2 \psi_0' + (e/m)\, r_0 A_0$ is an initial condition and the primes indicate differentiation with respect to time. In the system u, v, w, equs. (5) read

$$u'' = [-e/(m R^2)] \left[\frac{C}{R(1+u)} + (e/m) A\right] \cdot \left[-\frac{C m}{e R (1+u)^2} + \frac{\partial A}{\partial u}\right],$$
$$v'' = [-e/(m R^2)] \left[\frac{C}{R(1+u)} + (e/m) A\right] \frac{\partial A}{\partial v},$$
$$w' = \frac{1}{R^2 (1+u)^2} [C + (e R/m)(1+u) A], \qquad (6)$$
$$C = R^2 (1+u_0)^2 w_0 - (e/m) R (1+u_0) A_0 .$$

This transformation is performed by the relations:

$$u = (r - R)/R, \quad v = z/R, \quad w = \psi. \qquad (7)$$

The initial values of specific charge e/m, angular velocity w_0 and vector potential should be chosen such that the circle with radius R $(u = 0,\ v = 0)$ is a possible ion path. This may be achieved by using the EULER–LAGRANGE differential equations for the motion of a charged particle in a purely magnetic, w-independent field [7]:

$$\frac{d}{dw}\left(\frac{\partial F}{\partial u'}\right) - \frac{\partial F}{\partial u} = 0, \quad \frac{d}{dw}\left(\frac{\partial F}{\partial v'}\right) - \frac{\partial F}{\partial v} = 0, \qquad (8)$$

where

$$F(u, v, u', v') = \sqrt{(1+u)^2 + (u'^2 + v'^2)} - \eta (1+u)\, A_w \qquad (9)$$

is the ion-optical index of refraction for this special field. $\eta = \sqrt{e/(2 m U)}$ and U is the acceleration voltage of the ions. Expanding F into a power series up to the terms of the first order and substituting the first order approximation of A_w from (3) one gets

$$F = F_{00} + F_{10} u + \dots \text{ (terms of higher order in } u, v, u', v') \qquad (10)$$
$$= (1 - \tfrac{1}{2}\eta B) + (1 - \eta B)\, u + \dots .$$

The circle $u = 0$, $v = 0$ should be a possible ion path. From (10) and (8) follows:

$$F_{10} = 0 \quad \text{or} \quad \eta B = 1 . \qquad (11)$$

Let m_0 be the mass for which (11) holds and η_0 the corresponding value of η. Hence

$$\eta_0 B = 1 .$$

If the field strength B is normalized to unity one gets

$$\eta_0 = \sqrt{e/(m_0 2U)} = 1 . \qquad (12)$$

Here U may also be normalized to unity, yielding

$$e/m_0 = 2 . \qquad (13)$$

For an arbitrary mass m the normalized specific charge is

$$e/m = 2/p \qquad (14)$$

where $p = m/m_0$ is the ratio of an arbitrary mass and the mass for which $u = 0$, $v = 0$ is a possible trajectory.

The normalized linear velocity of a particle with mass m is taken from the relation

$$m c^2/2 = e U ,$$

therefore

$$c = \sqrt{2 e U/m} = \sqrt{2 e U/(m_0 p)} ;$$

taking the normalized values for U and e/m_0 yields

$$c = 2/\sqrt{p} . \qquad (15)$$

Hence, the normalized equations of motion read:

$$u'' = [-2/(p R^2)] \left[\frac{C}{R(1+u)} + (2/p) A\right] \cdot \left[-\frac{p C}{2 R (1+u)^2} + \frac{\partial A}{\partial u}\right],$$
$$v'' = [-2/(p R^2)] \left[\frac{C}{R(1+u)} + (2/p) A\right] \frac{\partial A}{\partial v},$$
$$w' = \frac{1}{R(1+u)} \left[\frac{C}{R(1+u)} + (2/p) A\right], \qquad (16)$$
$$C = R^2 (1+u_0)^2 w_0' - (2/p) R (1+u_0) A_0 .$$

Equs. (16) hold for positively charged particles only. According to (14), $-2/p$ should be taken instead of $+2/p$ for negatively charged particles. The circle $u = 0$, $v = 0$ is a possible trajectory with $p = 1$.

The normalized scalar and vector potentials follow directly from (1) and (3) by setting $B = 1$.

[10] L. S. GODDARD, Proc. Phys. Soc. London **56**, 372 [1944].

I.3. Integration of the Equations of Motion

Equs. (16) will now be integrated using a step by step method [10]. Let us consider an arbitrary value w_m of the azimuthal angle w, and suppose the corresponding values of the other coordinates of the particle,

$$w_m\,,\quad u_m\,,\quad v_m$$

to be known. Further, from the preceding step,

$$w'_{m-1'}\,,\qquad u_{m-1}\,,\qquad A_{m-1}$$

are known. First, from (16) the values of C which belongs to w_m is calculated:

$$C_m = R^2(1+u_{m-1})^2\, w'_{m-1} - (2/p)\, R(1+u_{m-1})\, A_{m-1}\,. \quad (17)$$

From (16) one gets the values of the second derivatives of u_m, v_m and the first derivative of w_m:

$$u''_m\,,\quad v''_m\,,\quad w'_m\,,$$

where A_m, $\partial A_m/\partial u$, $\partial A_m/\partial v$ have been calculated from (3).

In a small region around w_m, u_m, v_m, the values of u''_m, v''_m, may be taken as constant, and straightforward integration yields

$$u'_{m+1} = u'_m + u''_m \Delta t\,,\qquad v'_{m+1} = v'_m + v''_m \Delta t\,, \quad (18)$$

Δt being a short step of time, the precision of this approximation being the better the smaller the value of Δt. A second integration gives

$$\begin{aligned} u_{m+1} &= u_m + u'_m \Delta t + u''_m \Delta t^2/2\,,\\ v_{m+1} &= v_m + v'_m \Delta t + v''_m \Delta t^2/2\,,\\ w_{m+1} &= w_m + w' \Delta t\,. \end{aligned} \quad (19)$$

In this manner a particle trajectory starting from any initial condition may be traced with arbitrary precision throughout a purely magnetic field with rotational symmetry and an additional plane of symmetry.

I.4. Imaging Properties of Inhomogeneous Magnetic Sector Fields

Let us consider a hypothetical magnetic field which has the shape described in (1), within the sector $w=0$ and $w=\Phi$, and which is zero outside these boundaries. Therefore, in the following calculations, the stray fields are not accounted for. We have the case of an inhomogeneous magnetic sector field with plane boundaries and normal incident and exit of the mean path (fig. 3).

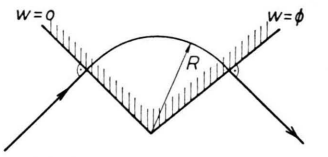

Fig. 3. Field Arrangement.

From fig. 4 a, b one takes the initial conditions at the object-sided field boundary $w=0$:

$$\begin{aligned} u_0 &= (1/R)\,(l\cdot \mathrm{tg}\,\alpha_m + \delta_x)\,,\\ v_0 &= (1/R)\,(l\cdot \mathrm{tg}\,\alpha_z + \delta_y)\,,\\ w_0 &= 0\,. \end{aligned} \quad (20)$$

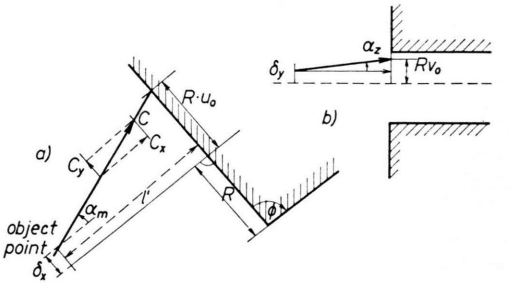

Fig. 4. Initial Conditions (Median Plane).

The components of the initial velocity c read (fig. 5)

$$\begin{aligned} c_x &= c\cdot \cos\alpha\cos\alpha_m\,,\\ c_y &= c\cdot \cos\alpha\sin\alpha_m\,,\\ c_z &= c\cdot \sin\alpha\,. \end{aligned} \quad (21)$$

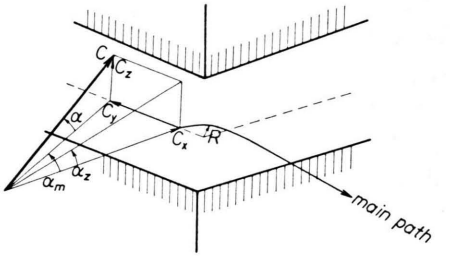

Fig. 5. Initial Conditions (Outside Median Plane).

α, α_m, α_z, being connected by the relation (fig. 5)

$$\mathrm{tg}\,\alpha = \mathrm{tg}\,\alpha_z \cos\alpha_m\,. \quad (22)$$

From (15), (20), (21), (22) one gets the normalized initial conditions:

$$\begin{aligned} u_0' &= (1/R)\; c_y = 2\cos\alpha\sin\alpha_m/(\sqrt{p}\,R)\,,\\ v_0' &= (1/R)\; c_z = 2\sin\alpha/(\sqrt{p}\,R)\,,\\ w_0' &= \frac{c_x}{R(1+u)} = 2\cos\alpha\cos\alpha_m/(\sqrt{p}\,R(1+u_0))\,. \end{aligned} \quad (23)$$

Using these initial conditions, the step by step integration is started. The iteration process terminates when for the first time a value $w_m \geq \Phi$ is obtained. Generally w does not assume the exact value $w = \Phi$. The values of the coordinates

$$u, u'; \quad v, v'; \quad w'$$

which correspond to $w = \Phi$ are obtained by linear interpolation between the last two iteration steps.

First we shall calculate the position of the GAUSSian image point corresponding to the object point with the coordinates $(l', 0, 0)$. This point is given by the intersection of a paraxial trajectory and the optical axis. Another possibility for the definition of the GAUSSian image point is the intersection of the beams with $\pm \alpha_G$.

$$x' = l', \qquad \delta_x = 0, \qquad \delta_y = 0,$$
$$\alpha_m = 0, \qquad \alpha_z = 0,$$
$$p = m/m_0.$$

According to our normalization, the optical axis for particles of mass m_0, i. e. $p = 1$ within the magnetic sector, is the circle with radius R in the median plane. In the field-free space it is formed by the rectilinear continuation of this circular path (fig. 6). For $p \neq 1$, the trajectories are noncircular, the coordinates at the exit boundary being

$$u = \bar{u}_\Phi, \quad v = 0, \quad \alpha_m = \bar{\alpha}_p, \quad \alpha_z = 0.$$

Trajectory 1 in fig. 6, therefore, is the optical axis for $m \neq m_0$. The corresponding paraxial trajectory is supposed to lie in the median plane, its object coordinates being

$$x' = l', \qquad \delta_x = 0, \quad \delta_y = 0,$$
$$\alpha_m = \alpha_G, \quad \alpha_z = 0,$$
$$p = m/m_0.$$

α_G should be a small angle for which

$$\sin \alpha_G \approx \operatorname{tg} \alpha_G \approx \alpha_G.$$

Trajectory 2 in fig. 6 is the paraxial ray for $m \neq m_0$. Its coordinates at the exit boundary are

$$u = u_{\Phi G}, \quad v = 0, \quad \alpha_m = \alpha_{\Phi G}, \quad \alpha_z = 0.$$

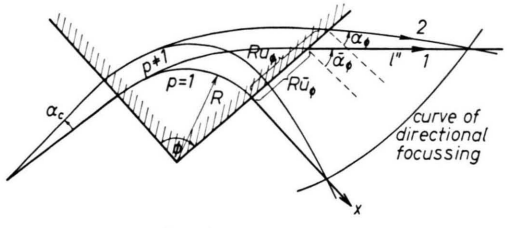

Fig. 6. Gaussian Optics for Different Masses.

From fig. 6 one takes the coordinates of the GAUSSian image point

$$x'' = l'' \cdot \cos \bar{\alpha}_\Phi,$$
$$y'' = R\,\bar{u}_\Phi + l'' \cdot \sin \bar{\alpha}_\Phi, \tag{24}$$

where the "image distance" l'' is given by

$$l'' = R(u_{\Phi G} - \bar{u}_\Phi) \cdot \cos \alpha_{\Phi G} / \sin(\bar{\alpha}_\Phi - \alpha_{\Phi G}). \tag{25}$$

At the image point given by (24), the aberrations of the imaging beam are calculated by finding the intersections of single trajectories with the perpendicular plane E to the optical axis in the GAUSSian image point. The intersection of any trajectory with plane E may be described by the two coordinates H, V (fig. 7).

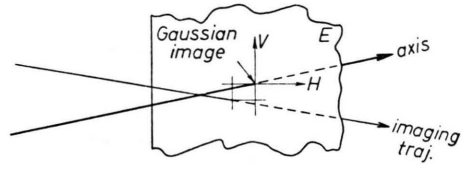

Fig. 7. Coordinate System for Aberrations.

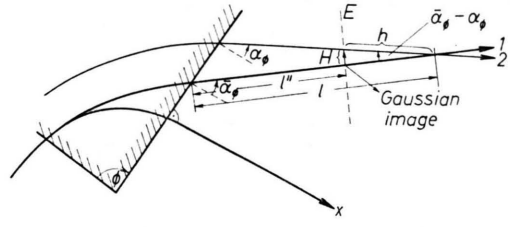

Fig. 8. Horizontal Aberration.

A trajectory (2 in fig. 8) from the imaging beam may have the coordinates

$$u_\Phi, \quad u'_\Phi, \quad v_\Phi, \quad v'_\Phi, \quad w'_\Phi$$

at the exit boundary. The horizontal and vertical angles of exit are

$$\operatorname{tg} \alpha_\Phi = u'_\Phi / [(1 + u_\Phi)\, w'_\Phi],$$
$$\operatorname{tg} \alpha_{z\Phi} = v'_\Phi / [(1 + u_\Phi)\, w'_\Phi]. \tag{26}$$

The projection of the trajectory (2 in fig. 8) intersects the axis (1 in fig. 8) of the beam at a distance l from the magnet boundary. Analogous to (25), l is given by

$$l = R(u_\Phi - \bar{u}_\Phi) \cos \alpha_\Phi / \sin(\bar{\alpha}_\Phi - \alpha_\Phi). \tag{27}$$

Again from fig. 8, the horizontal aberration is given by

$$H = (l - l'') \cdot \operatorname{tg}(\bar{\alpha}_\Phi - \alpha_\Phi). \tag{28}$$

The length of the projection of trajectory 2 in fig. 9 is

$$\bar{l} = l \cdot \cos \bar{\alpha}_\Phi / \cos \alpha_\Phi \,. \qquad (29)$$

The distance of the intersection of trajectory 2 with its projection from the magnet boundary, l_v, is given by (fig. 9):

$$l_v = -R\, v_\Phi / (\operatorname{tg} \alpha_{z\Phi} \cos \alpha_\Phi) \,. \qquad (29')$$

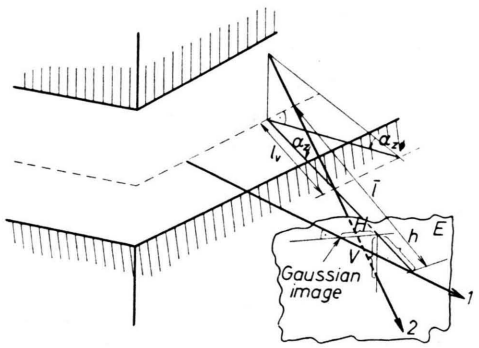

Fig. 9. Vertical Aberration.

Also, from fig. 8, one takes for the distance h:

$$h = (l - l'')/\cos(\bar{\alpha}_\Phi - \alpha_\Phi) \,, \qquad (30)$$

and for the vertical aberration with (29), (29′), (30)

$$V = (\bar{l} - l_v - h) \operatorname{tg} \alpha_z \,, \qquad (31)$$

where

$$\operatorname{tg} \alpha_z = \operatorname{tg} \alpha_{z\Phi} \cos \alpha_\Phi \quad \text{(see fig. 9)} \,. \qquad (32)$$

Calculation of the GAUSSian image point for various masses m yields the curve of directional focusing of the sector field. H and V give the geometrical aberrations in every point of that curve.

II. Results

In figs. 10 – 12, some graphs of the aberrations which have been calculated for different geometries are shown.

Fig. 10 shows the image of an infinitely narrow slit of 40 mm height. The inhomogeneity of the sector field is 0.5, the sector angle 169° 42′, and the mean radius 1 m, as realized in the SEIBERSDORF isotope separator [11]. In this case, the curve of direction focusing intersects the medium path at an angle

[11] F. P. VIEHBÖCK, Electromagnetic Separation of Radioactive Isotopes, Springer-Verlag, Wien 1961, p. 91.

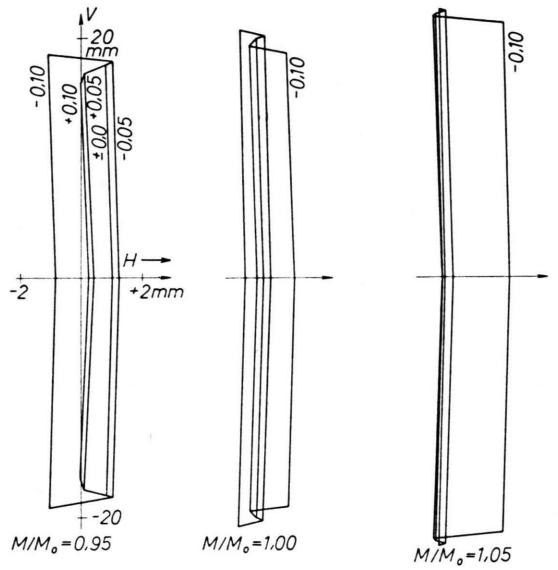

Fig. 10. $n = 0.5$, $\Phi = 169° 42'$. Second Order Angular Focusing, Stigmatic Focusing.

of about 34° and is curved slightly concave towards the magnet boundary. The graph shows the image shapes for mass lines of −5%, 0% and +5% mass deviation. The small symbols are the values of the horizontal opening angle, i. e. about −6, −3, 0, +3, +6 degrees. The vertical opening angle is always zero. One notices that the axial magnification increases slightly with increasing mass and equals unity at the medium path. An ion beam of 12 degrees total horizontal opening produces an image of 2 mm, 1.6 mm, 2.2 mm width for −5%, 0% and +5% mass deviation. The minimum image width at the medium path shows the second order focusing of the special field geometry. However, there is left a considerable third order contribution to the image width as may be noticed from the change of sign of the aberration as the opening angle passes through zero. If a total beam opening of 6 degrees is considered, the image widths for the same mass deviations are 1 mm, 0.4 mm and 0.4 mm, respectively. Thus, there is considerable image broadening with decreasing mass. At higher masses, focusing would be even better than in the second order focusing point except for the large negative angles.

Fig. 11 shows the axial focusing properties of the same setup. The horizontal opening here is zero, the vertical opening −6, −3, 0, +3, +6 degrees. A total vertical beam opening would result in an image width of about 8 mm. An opening of ±1.5 degrees

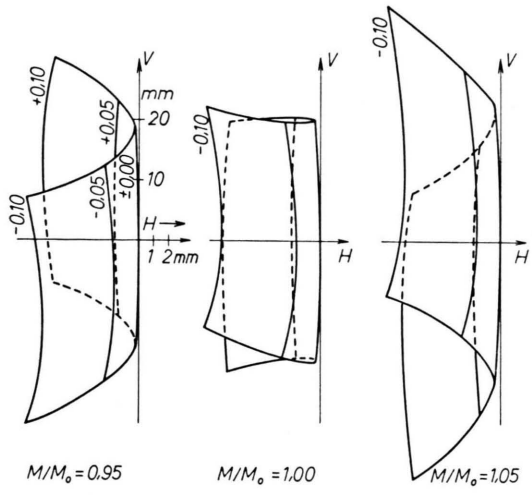

Fig. 11. $n=0.5$, $\Phi=169°\,42'$, $\alpha_m=0$. Agammatism, Sagittal Angular Aberration.

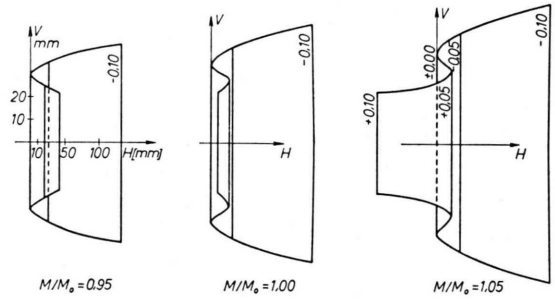

Fig. 12. $n=0.8$, $\Phi=180°$, $\alpha_z=0$, Symmetric Arrangement. Angular Aberration.

would give an image width of about 1 mm which may be tolerated in most cases. At the medium ion path there also occurs stigmatic focusing, whereas for higher masses as well as for lower masses a point source would exhibit considerable axial distortion.

Fig. 12 shows the aberrations of a field with a field index of 0.8 and a sector angle of 180 degrees. The pole shoe profile is conical, the mean radius again is 1 m, and image and object distance both are about 2.6 m. In this case the curve of axial focusing intersects the medium path at an angle of 20.5 degrees. Although this geometry gives a five-fold increase in dispersion compared with a homogeneous field with the same mean radius, this advantage is compensated by an extremely poor horizontal focusing action. A horizontal beam opening of ± 2 degrees results in an image width of about 22 mm, irrespective of the mass number. At such beam openings positive and negative angles equally contribute to the image broadening. In any case, if one wants to get a moderate image width with this geometry, the transmission of the instrument must be seriously reduced.

Acknowledgements

The authors wish to express their thanks to Mr. KERNTHALER and Mr. TATZBER for doing the programming work on the IBM 7040 and PB 250 electronic computers.